

Density Waves and Jet Emission Asymmetry in Bose FireworksHan Fu,^{1,*} Lei Feng,^{1,2} Brandon M. Anderson,³ Logan W. Clark,^{1,2} Jiazhong Hu,^{1,2}
Jeffery W. Andrade,⁴ Cheng Chin,^{1,2} and K. Levin¹¹*James Franck Institute, University of Chicago, Chicago, Illinois 60637, USA*²*Enrico Fermi Institute and Department of Physics, University of Chicago, Chicago, Illinois 60637, USA*³*Department of Computer Science, University of Chicago, Chicago, Illinois 60637, USA*⁴*Department of Physics, Harvard University, Cambridge, Massachusetts 02138, USA*

(Received 23 July 2018; published 11 December 2018)

A Bose condensate, subject to periodic modulation of the two-body interactions, was recently observed to emit matter-wave jets resembling fireworks [*Nature (London)* **551**, 356 (2017)]. In this Letter, combining experiment with numerical simulation, we demonstrate that these “Bose fireworks” represent a late stage in a complex time evolution of the driven condensate. We identify a “density wave” stage which precedes jet emission and results from the interference of matter waves. The density waves self-organize and self-amplify without breaking long range translational symmetry. This density wave structure deterministically establishes the template for the subsequent patterns of the emitted jets. Moreover, our simulations, in good agreement with experiment, address an apparent asymmetry in the jet pattern, and show that it is fully consistent with momentum conservation.

DOI: [10.1103/PhysRevLett.121.243001](https://doi.org/10.1103/PhysRevLett.121.243001)

Time-periodic driving, which allows coherent manipulation of many-body systems, is becoming an exciting tool in the field of ultracold atomic gases. Driving provides access to new quantum physics like, for example, topological states, synthetic gauge fields, and Mott transitions [1–7]. Of particular interest is the rather unique capability of these atomic systems to investigate nonequilibrium many-body dynamics [8]. Also unique to ultracold gases is the ability to use Feshbach resonances to periodically modulate atomic interactions [9], as recently implemented by the Chicago group [10,11] and the Rice group [12–14] on Bose-Einstein condensates (BECs). In the Chicago experiment, a collective emission of matter-wave jets resembling fireworks occurs above a threshold modulation amplitude [10].

In the present Letter, we use the time-dependent Gross-Pitaevskii (GP) equation to study the evolution of the modulated BECs and the emission of jets. We show that the simulations reliably capture the “Bose fireworks” dynamics seen in experiments. In combination with a new set of experiments, we identify a previously unobserved early stage of the time evolution. Immediately after the onset of modulation, we observe that density waves emerge and grow rapidly within the condensate. The density waves display a high degree of disorder, reflecting quantum fluctuations that we model with a very small [15] random noise term.

As in general parametric resonances [16–20], the density waves set up an effective, self-consistently produced “grating” that, through feed-back effects, resonantly amplifies their pattern [21]. (A notable feature distinguishing the parametric resonance here is that the amplification can occur with an essentially arbitrary driving frequency.)

This process proceeds until pairs of jets (having wave number determined by [10,22] the modulation frequency ω) are ejected in opposite directions. Within these pairwise correlations, there remains a quantitative asymmetry that has attracted prior attention [23,24].

We focus on two important results: first, we show that the density wave pattern underlies the jet-emission process, and second, we provide a quantitative understanding of the puzzling asymmetry in the emission pattern. Figure 1 summarizes the full evolution of the system, and it shows good agreement between our simulations and experiment. Three distinct regimes of the Bose fireworks can be identified: the early density wave (DW) regime, the initial emergence of jets (called the “near-field emission”) and the well established jet emission regime (called the “far-field emission”). In the near-field stage, the excited modes begin to leave the condensate while still substantially overlapping with each other. After a sufficiently long time, the matter-wave jets become well separated in the far field, and the observed density profiles primarily reflect the populations in momentum-space.

We begin with the theoretical and experimental investigation of the early-stage density waves. Figure 2 presents the experimental observation and theoretical confirmation of the emergence of density waves. The experiments begin with a Bose condensate of 4×10^4 cesium atoms prepared in a uniform disk-shaped trap with a radius of $13 \mu\text{m}$ (see Ref. [10] for experimental details). The trap has a potential barrier of height $h \times 200$ Hz in the horizontal direction (h is the Planck constant) and is harmonic vertically, with a frequency of 220 Hz. By modulating the magnetic field

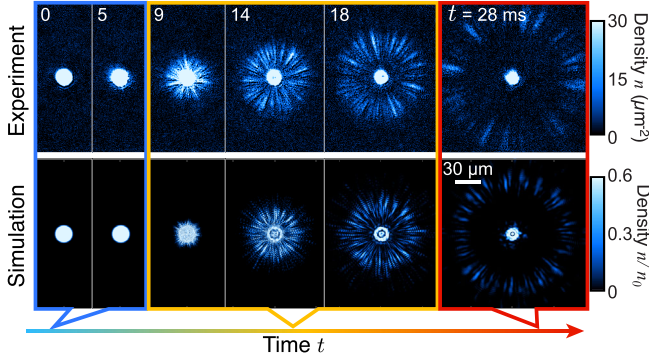


FIG. 1. The real space density distribution $n(\mathbf{r})$ as a comparison between experimental data and simulations. In both, the modulation frequency, $\omega/2\pi$, is 2 kHz and the dc and ac interaction energies, respectively, are $U_0 n_0 \approx h \times 40$ Hz and $U_1 n_0 \approx h \times 480$ Hz, where h is Planck's constant (see the main text for detailed definitions). As a function of modulation time t , the system exhibits three phases: density waves in a confined condensate (blue box), near-field emission (orange box), and far-field emission (red box).

near a Feshbach resonance, we make the scattering length oscillate as $a(t) = a_{\text{dc}} + a_{\text{ac}} \sin(\omega t)$ with a small offset, $a_{\text{dc}} = 4a_0$, and a large amplitude, $a_{\text{ac}} = 40a_0$, at frequency $\omega/2\pi = 620$ Hz, where a_0 is the Bohr radius.

After modulating the interaction for time t , we perform *in situ* imaging and observe density waves forming within the condensate prior to jet emission. Figure 2(a) shows snapshots of the condensate density distribution $n(\mathbf{r})$ and theoretical simulations. To be more quantitative, we extract the density wave amplitude, $A_{k_f} = n_0^{-1} \int_{|\mathbf{k}|=k_f} d\mathbf{k} |\tilde{n}(\mathbf{k})|$, from the Fourier transformation of the condensate density, $\tilde{n}(\mathbf{k}) = (2\pi)^{-1} \int d\mathbf{r} e^{-i\mathbf{k}\cdot\mathbf{r}} n(\mathbf{r})$, see Fig. 2(b). Here, $k_f = \sqrt{m\omega/\hbar}$ is the wave number of the density wave determined by the parametric resonance condition, n_0 is the average density of the static condensate prior to interaction oscillations, m is the boson mass, and \hbar is the reduced Planck constant. Interestingly, this density wave amplitude exhibits fast oscillation under a slowly growing envelope.

We note that, this density wave pattern is reminiscent of Faraday waves in classical fluids [25,26], and is related to that predicted for driven atomic gases [27–30] as well as observed in a one-dimensional condensate [31]. In contrast to classical Faraday waves, our system does not spontaneously exhibit threefold or higher symmetries. These symmetries are expected to arise from nonlinear kinetic terms in the hydrodynamic equations of motion [25,26], which are not present in the GP equation.

Our theoretical approach is based on a dynamical GP equation:

$$i\hbar \frac{\partial \psi}{\partial t} = \left(-\frac{\hbar^2}{2m} \nabla^2 + V(\mathbf{r}) + U_0 |\psi|^2 - \mu \right) \psi + U_1 \sin(\omega t) |\psi|^2 \psi, \quad (1)$$

where ψ is the wave function, $\mu = U_0 n_0$ is the chemical potential of the static condensate, $V(\mathbf{r})$ is the external trap potential, and $\mathbf{r} = (x, y)$ is a two-dimensional (2D) spatial coordinate (with origin at the trap center). In addition, $U_0 = 4\pi\hbar^2 a_{\text{dc}}/m$ and $U_1 = 4\pi\hbar^2 a_{\text{ac}}/m$ are the dc and ac interaction strengths, respectively. At short times, the condensate is weakly excited and the wave function can be linearized [27,28]

$$\psi = \psi_0 [1 + \nu(\mathbf{r}, t)], \quad (2)$$

where $\psi_0 = \sqrt{n_0} \exp[iU_1 n_0 \cos(\omega t)/\hbar\omega]$ is the wave function of a uniform BEC, and U_0 has been absorbed through the parametrization in Eq. (1). Since the characteristic DW length scales are much smaller than the trap size, we ignore trap effects in our analytical approach. In the plane wave basis, we write $\nu(\mathbf{r}, t) = [\xi(t) + i\zeta(t)] \cos(\mathbf{k} \cdot \mathbf{r} + \varphi)$ with both $\xi(t)$ and $\zeta(t)$ real and φ a random phase. Since $|\nu| \ll 1$, ξ satisfies the Mathieu equation for parametric resonances:

$$\frac{\partial^2 \xi}{\partial t^2} + \Omega^2 [1 + \alpha \sin(\omega t)] \xi = 0, \quad (3)$$

and ζ satisfies the same equation with an extra term $-\alpha\omega \cos(\omega t) (\partial \zeta / \partial t)$ on the left-hand side. Here, we keep only the leading terms in α , $\Omega^2 = \hbar^2 k^4 / 4m^2 + U_0 n_0 k^2 / m$, and $\alpha = U_1 n_0 k^2 / m\Omega^2$.

The solution of Eq. (3) is $\xi(t) \approx A_+ \cos(\omega t/2 + \vartheta_+) \exp(\lambda_+ t) + A_- \sin(\omega t/2 + \vartheta_-) \exp(\lambda_- t)$. Here, A_{\pm} are numerical coefficients, and the exponents are

$$\lambda_{\pm} = \pm \sqrt{\frac{\alpha^2 \Omega^2}{16} - \left(\Omega - \frac{\omega}{2} \right)^2}. \quad (4)$$

The solution exhibits both subharmonic oscillations with half the driving frequency, ω , and an exponential envelope growth (via λ_+). For $U_0 \approx 0$, as in the experiments, the resonance with maximal λ_+ occurs at $k = k_f$. At this point, $\vartheta_{\pm} \approx 0$ and $\zeta(t) \approx -A_+ \sin(\omega t/2) \exp(\lambda_+ t) + A_- \cos(\omega t/2) \exp(\lambda_- t)$.

The interference between the uniform background and the excitations then gives the density $n(\mathbf{r}) = n_0 |1 + \nu(\mathbf{r}, t)|^2 \approx n_0 [1 + 2\xi(t) \cos(\mathbf{k} \cdot \mathbf{r} + \varphi)]$, leading to the density waves of the exponentially growing envelope that we report here. To provide the full dynamical evolution and to include trap effects, we next appeal to the more complete numerical simulations of the GP equation.

Our simulations are 2D, and they incorporate a ring trap with inner and outer radii, R_{in} and R_{out} , respectively. We choose $V(\mathbf{r}) = V_0$ for $R_{\text{in}} < r < R_{\text{out}}$ and zero elsewhere. V_0 is taken to be compatible with experiment, R_{in} is taken to be the condensate radius, and, as in experiment [10], $R_{\text{out}} \approx 1.5R_{\text{in}}$. We use a CUDA-based GP equation solver [32,33], implemented on graphic processing units, based on a split-step algorithm. At $t > 0$, we introduce a periodic oscillation of the two-body interaction term.

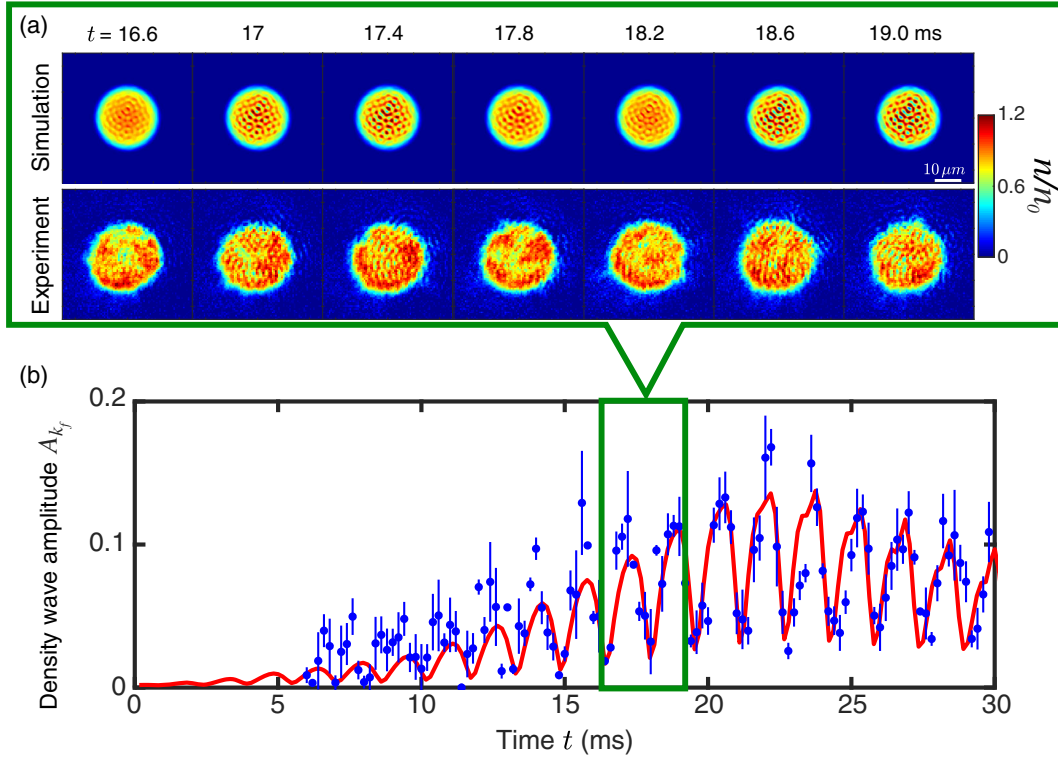


FIG. 2. Experiment and simulation comparison for early-stage density waves (DW) with $|k| = k_f$. (a) The real-space DW oscillations inside the condensate. Theory (top) and experiment (bottom) show good qualitative agreement. The experiment exhibits additional static, long-wavelength density modulations due to trap imperfections. The experimental details are provided in the main text. (b) The amplitude of the density waves in the primary mode comparing simulations (red solid line) and experiments (blue dots with error bars). In addition to fast oscillations, both results show a consistent observation of an exponential growth of the envelope until the matter-wave jets are emitted from the condensate.

It should be noted that the exponents in Eq. (4) coincide with those derived in Ref. [10] for the matter-wave jets. This suggests that the two forms of excitations may be manifestations of the same physics. We probe this hypothesis in Fig. 3, which contains results from our full GP simulations. Indeed, Fig. 3 provides strong simulation evidence that the density waves are necessary precursors to the jets, and that they establish the template for the subsequent jet emission pattern. In particular, we find that the structure factor with fixed extrema (established by the DW pattern at the onset of shaking) is precisely equivalent to the real-space emitted jet population $N(\phi)$ observed after a long propagation time.

The structure factor is defined by $S(k_f, \phi) = N_0^{-1} \int k dk |\tilde{n}(\mathbf{k})|^2$, where the magnitude and phase of the wave vector are $|\mathbf{k}| = k \approx k_f$ and $\phi = \arctan(k_x/k_y)$. Note from Fig. 3(a) that the structure factor contains random peaks and valleys as determined by the initial random seed which emulates the fluctuations of real experiments. These patterns are established at the onset of shaking, and the only change with increasing time is an exponential growth of the peak amplitudes.

The dashed black line plotted in Fig. 3(a) is the real-space azimuthal distribution for the jet population

$N(\phi) = \int_{\mathbf{r}=(\hbar t/m)\mathbf{k}} r dr n(\mathbf{r})$, at long times. Importantly, the angular distribution shows the equivalence between $S(k_f, \phi)$ and $N(\phi)$. This underlies our claim that density waves and jets are deterministically correlated. These results are summarized in Fig. 3(b). This presents a schematic plot linking the momentum space spectrum of the DW and the population of jets with the same wave vector $\pm\mathbf{k}$ after long time of flight.

Having established the equivalence between the far-field jets and the initial density waves, one might expect that the same azimuthal distribution would appear in the near-field regime, when jets are first emitted from the condensate. However, our simulations show that this is not the case. In Figs. 4(a) and 4(b), a clear modification of the distribution shape with varying time is seen, and is accompanied by an “inversion symmetry breaking” (in the near field). This is associated with the observation (reported experimentally [10]) of an asymmetric two-particle correlation function $g^{(2)}(\phi)$ of the jet emission pattern, i.e., $g^{(2)}(\pi) \neq g^{(2)}(0)$.

Here, we propose and provide strong numerical support for a scenario that explains this observation. Moreover, in contrast to the literature [23,24], in our scenario, momentum is fully conserved. This is well substantiated by the detailed numerics summarized in Fig. 4(c), along with analytical

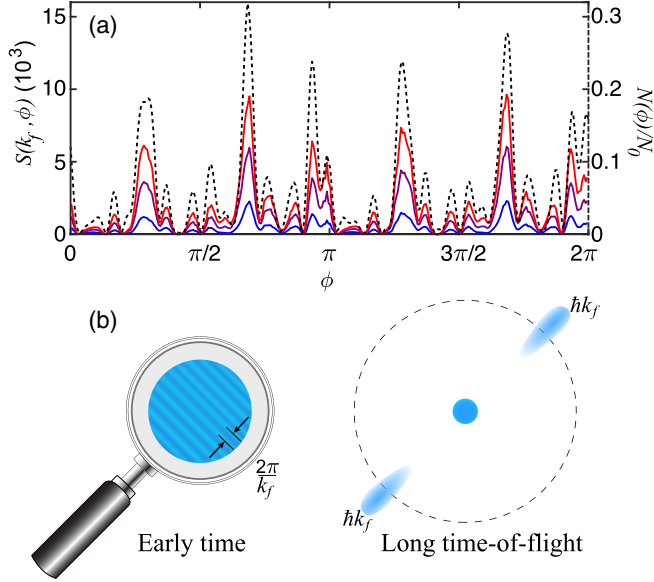


FIG. 3. Connection between density waves before jet emission and the subsequent matter-wave jet pattern. (a) shows the azimuthal density structure factor $S(k_f)$ from a single iteration of the GP simulations at the resonant wave number k_f at $t = 10$ (blue), 13 (purple), and 15 (red) ms prior to jet emission. At each time, we observe the same shape with a growing amplitude, consistent with the expected amplification process of density waves. The dashed black curve is the real-space azimuthal population distribution of jets $N(\phi)$ at $t = 45$ ms. The scaling factor, N_0 , is the total number of atoms in the system. The alignment of all maxima and minima between $S(k_f, \phi)$ and $N(\phi)$ shows the equivalence between the density waves and jets. (b) schematically shows that the early-time density waves with wave number k_f leads to the emission of counter-propagating jets with the same wave number k_f at the long time.

arguments in the Supplemental Material [34]. To quantify this inversion asymmetry, we introduce a parameter,

$$\eta_r = \frac{\langle [N(\theta) - N(\theta + \pi)]^2 \rangle}{2\langle N(\theta) \rangle^2} = g^{(2)}(0) - g^{(2)}(\pi),$$

for real space (and its analogue, η_k in momentum space [34]), where $\langle \dots \rangle$ corresponds to averaging over angles θ and ensembles. Figure 4(c) plots the asymmetry functions, $\eta_{r,k}$, in real- and momentum-space, together with the corresponding correlation function $g^{(2)}(\phi)$ shown in the inset. The spatial asymmetry η_r decreases from a finite value to zero when going from the near to far field. This indicates that the inversion symmetry is recovered at large times. The momentum-space asymmetry, η_k , interestingly, remains zero independent of time, showing clearly that momentum conservation is obeyed at all times.

We attribute this asymmetry to the fact that, in the near field, excitations of different wave vectors substantially overlap with each other. The resulting pattern is derived from the interference between these overlapping modes, which have uncorrelated random phases. Thus, when

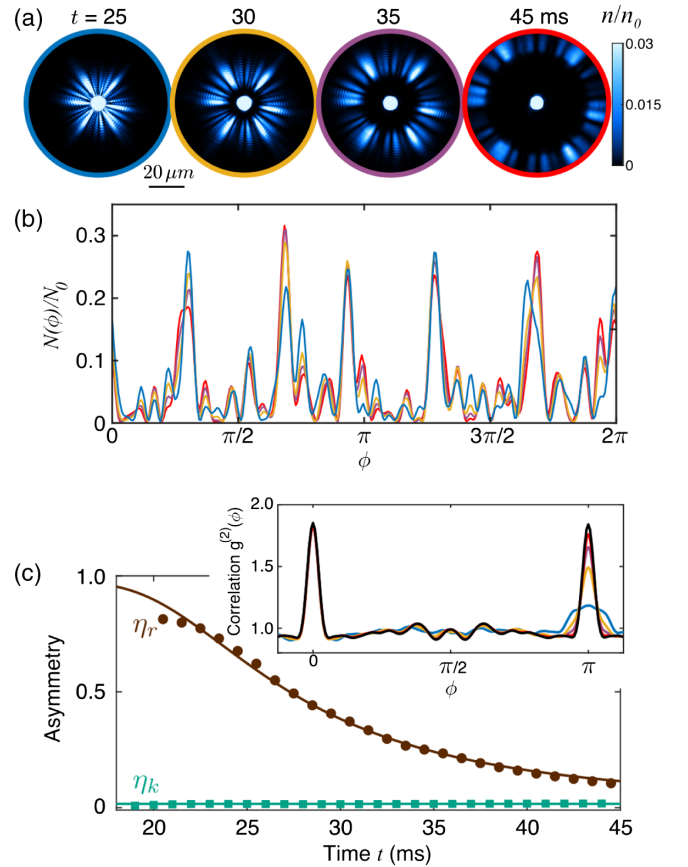


FIG. 4. Time evolution and correlations of the emitted jets. (a) shows the calculated jet emission pattern evolving from the near- to far-field regimes. The calculation is based on identical initial noise seeding. (b) shows the real space azimuthal population of the four images in (a), identified by the same color. Note that, the $t = 45$ ms far-field curve is equivalent to that shown dashed in Fig. 3(a). Here, unlike in Fig. 3, the peaks and valleys are slightly displaced with time. Panel (c) probes the emission asymmetry in real space $\eta_r = g^{(2)}(\pi) - g^{(2)}(0)$ (brown circles) and the momentum-space analogue η_k (green squares). The main figure shows that the $(0, \pi)$ asymmetry is always absent in momentum space (η_k is strictly zero within numerical precision) so that momentum is conserved. In real space, using (b), we find that this $(0, \pi)$ asymmetry decreases with increasing time. The inset indicates the correlation function $g^{(2)}(\phi)$ at the same four times as in (a), along with an early time momentum correlation function at $t = 20$ ms (black curve). Again, inversion $0 - \pi$ symmetry is broken at short times, but it recovers after a long time-of-flight and is fully preserved in momentum space. The solid line (brown) in (c) is an analytical fit to η_r [34].

measuring the population at angles θ and $\theta + \pi$, the symmetry between the relevant counter-propagating pair $\pm \mathbf{k}$ ($\tan \theta = k_y/k_x$) is masked by interference from other uncorrelated modes. By contrast, in the far field, different modes are well separated so that each jet now represents a single mode. Here, momentum conservation is more apparent and inversion symmetry in real space is recovered [34].

The asymmetry in the emission pattern has alternatively been attributed to di-jet acollinearity due to hydrodynamic collisions, seen, for example, in quark-gluon plasmas [23], or to the Hanbury Brown–Twiss effect in the angular momentum eigenstate basis within a time-dependent Bogoliubov theory [24]. In this context, our numerical calculations show that momentum conservation persists throughout the entire evolution, as argued earlier [10]. In this Letter, we have provided a more intuitive and quantitative picture showing how the asymmetry arises from the interference between overlapping matter-wave modes [34].

Conclusions.—The present Letter has addressed the jet emission process induced by a periodic drive of the two-body interactions. Through a combination of simulations of the Gross-Pitaevskii equation and experiments, we demonstrated that the jet structure is imprinted in the early stages of an excited condensate through density waves. Observing the actual density waves in experiments, as reported in the present Letter, was key to confirming this picture. Also critical to this analysis is the demonstrated capability of the GP simulations. They have successfully addressed stimulated emission experiments over widely varying time, space, and momentum coordinates. Our simulations have provided predictive capabilities as well as the ability to establish the important underlying principles (such as momentum conservation) of a broad scope of experimental matter-wave jet observations.

We are grateful to Tom Witten for helpful discussions and Igor Aronson and Andreas Glatz for the numerical GP code. L.F. acknowledges support from an MRSEC-funded Graduate Research Fellowship. L.W.C. was supported by a Grainger Graduate Fellowship. This work was primarily supported by the University of Chicago Materials Research Science and Engineering Center, which is funded by the National Science Foundation under Grant No. DMR-1420709. We also acknowledge support from NSF Grant No. PHY-1511696 and the Army Research Office-Multidisciplinary Research Initiative under Grant No. W911NF-14-1-0003.

*Corresponding author.

vickeyrobert@uchicago.edu

- [1] A. Eckardt, *Rev. Mod. Phys.* **89**, 011004 (2017).
- [2] G. Jotzu, M. Messer, R. Desbuquois, M. Lebrat, T. Uehlinger, D. Greif, and T. Esslinger, *Nature (London)* **515**, 237 (2014).
- [3] M. Aidelsburger, M. Lohse, C. Schweizer, M. Atala, J. T. Barreiro, S. Nascimbène, N. R. Cooper, I. Bloch, and N. Goldman, *Nat. Phys.* **11**, 162 (2015).
- [4] M. Aidelsburger, M. Atala, S. Nascimbène, S. Trotzky, Y.-A. Chen, and I. Bloch, *Phys. Rev. Lett.* **107**, 255301 (2011).
- [5] A. Zenesini, H. Lignier, D. Ciampini, O. Morsch, and E. Arimondo, *Phys. Rev. Lett.* **102**, 100403 (2009).
- [6] J. Dalibard, F. Gerbier, G. Juzeliūnas, and P. Öhberg, *Rev. Mod. Phys.* **83**, 1523 (2011).
- [7] E. J. Mueller, *Phys. Rev. A* **70**, 041603 (2004).
- [8] A. Polkovnikov, K. Sengupta, A. Silva, and M. Vengalattore, *Rev. Mod. Phys.* **83**, 863 (2011).
- [9] C. Chin, R. Grimm, P. Julienne, and E. Tiesinga, *Rev. Mod. Phys.* **82**, 1225 (2010).
- [10] L. W. Clark, A. Gaj, L. Feng, and C. Chin, *Nature (London)* **551**, 356 (2017).
- [11] L. W. Clark, B. M. Anderson, L. Feng, A. Gaj, K. Levin, and C. Chin, *Phys. Rev. Lett.* **121**, 030402 (2018).
- [12] S. E. Pollack, D. Dries, M. Junker, Y. P. Chen, T. A. Corcovilos, and R. G. Hulet, *Phys. Rev. Lett.* **102**, 090402 (2009).
- [13] S. E. Pollack, D. Dries, R. G. Hulet, K. M. F. Magalhães, E. A. L. Henn, E. R. F. Ramos, M. A. Caracanhas, and V. S. Bagnato, *Phys. Rev. A* **81**, 053627 (2010).
- [14] M. C. Tsatsos, J. H. V. Nguyen, A. U. J. Lode, G. D. Telles, D. Luo, V. S. Bagnato, and R. G. Hulet, [arXiv:1707.04055](https://arxiv.org/abs/1707.04055).
- [15] The fluctuation term $\psi_s = \epsilon_r + i\epsilon_i$ is added to the initial ground state wave function ψ_0 . Here, we chose the random variables ϵ_r and ϵ_i to have a Gaussian probability density function centered around zero with standard deviation $\sigma = 0.1|\psi_0|$.
- [16] S. Lellouch, M. Bukov, E. Demler, and N. Goldman, *Phys. Rev. X* **7**, 021015 (2017).
- [17] M. Krämer, C. Tozzo, and F. Dalfovo, *Phys. Rev. A* **71**, 061602 (2005).
- [18] G. K. Campbell, J. Mun, M. Boyd, E. W. Streed, W. Ketterle, and D. E. Pritchard, *Phys. Rev. Lett.* **96**, 020406 (2006).
- [19] N. Gemelke, E. Sarajlic, Y. Bidel, S. Hong, and S. Chu, *Phys. Rev. Lett.* **95**, 170404 (2005).
- [20] L. Fallani, L. De Sarlo, J. E. Lye, M. Modugno, R. Saers, C. Fort, and M. Inguscio, *Phys. Rev. Lett.* **93**, 140406 (2004).
- [21] S. Inouye, A. P. Chikkatur, D. M. Stamper-Kurn, J. Stenger, D. E. Pritchard, and W. Ketterle, *Science* **285**, 571 (1999).
- [22] L. Feng, J. Hu, L. W. Clark, and C. Chin, [arXiv:1803.01786](https://arxiv.org/abs/1803.01786).
- [23] M. Arratia, [arXiv:1801.05515](https://arxiv.org/abs/1801.05515).
- [24] Z. Wu and H. Zhai, [arXiv:1804.08251](https://arxiv.org/abs/1804.08251).
- [25] S. T. Milner, *J. Fluid Mech.* **225**, 81 (1991).
- [26] W. Zhang and J. Viñals, *J. Fluid Mech.* **336**, 301 (1997).
- [27] K. Staliūnas, S. Longhi, and G. J. de Valcárcel, *Phys. Rev. Lett.* **89**, 210406 (2002).
- [28] Y. Kagan and L. Manakova, *Phys. Lett. A* **361**, 401 (2007).
- [29] A. I. Nicolin, R. Carretero-González, and P. G. Kevrekidis, *Phys. Rev. A* **76**, 063609 (2007).
- [30] A. Balaž, R. Paun, A. I. Nicolin, S. Balasubramanian, and R. Ramaswamy, *Phys. Rev. A* **89**, 023609 (2014).
- [31] P. Engels, C. Atherton, and M. A. Hoefer, *Phys. Rev. Lett.* **98**, 095301 (2007).
- [32] P. Scherpelz, K. Padavić, A. Rançon, A. Glatz, I. S. Aranson, and K. Levin, *Phys. Rev. Lett.* **113**, 125301 (2014).
- [33] B. M. Anderson, L. W. Clark, J. Crawford, A. Glatz, I. S. Aranson, P. Scherpelz, L. Feng, C. Chin, and K. Levin, *Phys. Rev. Lett.* **118**, 220401 (2017).
- [34] See Supplemental Material at <http://link.aps.org/supplemental/10.1103/PhysRevLett.121.243001> for more numerical evidence on momentum conservation and analytical arguments on interference-caused near-field asymmetry.